

Preparation and characterization of rubber-lead nanocomposite material as a protective shield against cobalt gamma radiation

F. K. Dahash¹, A. K. Aobaid², E. Koç³, A. N. Saud^{4,*}, M. H. Al Maamori⁵

¹ College of Pharmacy, University of AL-Qadisiya, AL-Qadisiya 58002, Iraq

² Department of Physics, University of Anbar, Anbar 31001, Iraq.

³ Department of Biomedical Engineering, Karabük University, Karabük 78050, Turkey

⁴ Biomedical Engineering, Al-Mustaqbal University College, Babylon 51002 Iraq

⁵ Prosthetics & orthotics Engineering, Al-Mustaqbal University College, Babylon 51002 Iraq

The current study investigates the potential of styrene-butadiene rubber (SBR) nanocomposite reinforced with nano-lead (N-Pb) as a protective shield against gamma radiation emitted from a Cobalt-60 (Co-60) source. The influence of varying N-Pb concentrations (50–300 parts per hundred parts of rubber, pphr) on the structural, morphological, and radiation-shielding characteristics was investigated. The nanocomposite was characterized using several analytical techniques, including X-ray diffraction (XRD), Fourier transform infrared spectroscopy (FTIR), and scanning electron microscopy (SEM). The results demonstrate that increasing the N-Pb concentration leads to enhanced crystallinity, improved homogeneity, and significantly enhanced gamma radiation shielding capabilities of the material. Notably, the nanocomposite exhibited a substantial decrease in gamma count rate (31.9% reduction with 300 pphr N-Pb), mean free path (81% decrease), half-value layer (77% decrease), and tenth-value layer (87% decrease) as the N-Pb content increased. These findings highlight the promising potential of SBR-N-Pb nanocomposites as a cost-effective and efficient shielding material for various gamma radiation applications.

(Received November 29, 2024; Accepted February 27, 2025)

Keywords: Styrene-butadiene rubber, Gamma radiation shielding, Attenuation coefficients, Polymers nanocomposites, Nuclear applications

1. Introduction

The rising prevalence of cancer, coupled with the expanding applications of nuclear technology, has underscored the urgency for developing effective radiation protection solutions [1]. Among the various forms of radiation, gamma rays and high-energy electromagnetic radiation are particularly pernicious due to their deep penetration capabilities, posing significant risks to medical personnel and patients undergoing radiotherapy and workers in nuclear facilities [2]. The most crucial use of gamma rays in medicine is the diagnosis and treatment of injuries, especially the treatment of cancerous tissue. It kills precancerous cells and prevents them from growing as these rays penetrate the skin and ionize cells, killing the cell's lead [3]. It is also used to treat eyes, increase thyroid secretion, and sterilize medical instruments through radiation. During the regular treatment of patients with tumours, the standard, unaffected tissues of the patient and those treating them are exposed to harmful radiation. For this purpose, suitable protective materials must be used to avoid damage to the healthy tissue of patients and employees in tumour centers [4].

Effective radiation shielding materials are essential for ensuring the safe use of ionizing radiation technologies, such as those involving gamma rays and radioactive isotopes. Continued advancements in nuclear radiation protection emphasize the development of enhanced shielding solutions, highlighting the increasing relevance of this area of research. One of the contemporary advancements in shielding materials is the development of "transparent shielding polymers." These materials incorporate a percentage of highly efficient nanoparticles into standard transparent

* Corresponding author: amir.saud92@gmail.com

<https://doi.org/10.15251/DJNB.2025.201.239>

polymers, resulting in enhanced optical and radiation shielding properties [5, 6]. Recently, a novel radiation shielding material, composed of polyurethane and polyvinyl chloride reinforced with heavy metal salts (e.g., lead and barium), has been developed; this composite, offering protection against X-rays and gamma rays, represents a significant advancement in radiation protection technology[7].

The composite materials made of polymer and metal, or ceramic, have improved physical properties such as (thermal conductivity, mechanical, optical, magnetic, and electrical). Some studies focus on creating composite materials by integrating various fillers into different matrices, aiming to combine their properties into a single effective radiation shield [8].

Polymer-based nanocomposites are being developed for radiation shielding applications. The high surface area of the nanoparticles, coupled with the flexibility and durability of the polymer, results in lightweight and effective radiation barriers. Moreover, silicon rubber matrices combined with various nanomaterials have been shown to improve the gamma radiation attenuation capabilities of these nanocomposite shielding solutions. These engineered composites' uniform dispersion and reduced internal stresses enhance their protective performance [8, 9].

Recent studies have investigated the radiation-shielding capabilities of polymer nanomaterials; Ibrahim et al.[10] studied the physical properties of styrene-butadiene rubber solutions in heptane before and after exposure to gamma radiation from a Co-60 source with an energy of 1.22 MeV and a radiation dose of 255.08 Rad. The research involved calculating various rheological properties, such as viscosity and revealed a decrease in density values following irradiation. Shruti et al. [11] explored the radiation shielding effectiveness of a nanocomposite consisting of nanomethylsiloxane and bismuth oxide. Their findings demonstrated that a composite containing 44.44% bismuth oxide nanoparticles attenuated X-rays at 60 kilovolts with a thickness of 3.73 mm. Badawy et al.[12] developed a polyvinyl alcohol (PVA)/magnetic materials nanocomposite, which exhibited enhanced radiation shielding properties. This improvement was attributed to the lower saturation magnetization of the magnetic materials (MS) than that of pure magnetite and the superconductive behavior of PVA at room temperature. Al-Qaisi and Aobaid [13] investigated the impact of gamma radiation from a Co-60 source on the thermal conductivity of an epoxy resin reinforced with SiC nanoceramic and a hybrid SiC-graphite material with weight fractions of 2%, 4%, and 6%. Their results indicated that thermal conductivity increases with higher weight fractions before irradiation. However, due to the superior conductivity of the graphite reinforcing material compared to silicon, the thermal conductivity values further increased after irradiation with doses of 6, 8, and 10 KGy. El-Khatib et al. [14] examined the morphological properties and attenuation coefficients for gamma radiation protection in dimethylpolysiloxane mixed with micro- and nano-sized PbO at different weight ratios. Their research found that increasing the proportion of lead oxide filler significantly enhanced the linear attenuation coefficient and improved radiation shielding parameters, particularly at lower gamma energies.

Furthermore, the study indicated that using nano-sized lead oxide in the silicone rubber (SR) matrix resulted in superior radiation shielding performance. Rola et al. [15] investigated the relationship between the cutting connection of the memory formation density of the vulcanized natural rubber (SMNR) with different sulphur contents in the range (0.75-2)pphr, and the results showed that the increased crosslinking negatively impacted the shape memory properties of the "smart" rubber material. Compared to lead monoxide, PbO exhibits superior performance over the other lead oxides[16]. Rubber-lead mixtures were highly flexible and homogeneous, and their radiation protection properties improved with increasing lead concentrations [17]. By reinforcing the SBR matrix with various loading ratios of Pb-NPs and additional additives, like chlorophyll and TiO₂, this study aims to create practical barriers to ionizing radiation and increase safety for medical personnel, patients, and workers at nuclear facilities. These improvements include increased crosslink density, improved resistance to oxidation, and increased rubber compound efficiency for shielding against gamma rays.

2. Experimental practical

2.1 Preparation of samples

A polymeric composite master batch preparation involved meticulously mixing the materials using a laboratory mill equipped with rolls measuring 150mm on the outside and a working distance of 300mm. The slow roll operated at 24 rpm, and the mill facilitated precise control over the gap distance between the rolls. The ingredients were carefully added according to the standard IT1060 specifications, following the formulation outlined in Table 1. The processing recipe for the master batch incorporated varying mixing times. The mixing and homogenization process proceeds: The styrene-butadiene rubber (SBR) was passed between the rollers several times. At the same time, the opening between the two rollers was reduced. This process is carried out at a temperature of 45°C. Stearic acid was then added at a rate of 1.75 pphr and continuously mixed with the rubber between the rollers. Then zinc oxide and titanium oxide were added at a rate of 0.6 and 20 pphr, respectively. Twenty pphr of Chlorophyll was added by extracting it from the plant (Alfalfa) using acetone as solvent [18]. The accelerator TMTD was added at 0.6 pphr and sulphur at 2.6 pphr to ensure the temperature does not exceed 45°C. Then, nano-lead is added in a different ratio, as shown in Table 1. Roll the batch around the two rolls several times while reducing the hole to 0.28 mm for final homogenization, then cool to room temperature and let stand for 24 hours to avoid internal stress to remove the characterizations.

Table 1. The compounding of the rubber nanocomposites.

Compounding ingredients	pphr	Manufacturer
SBR	100	Synthos S.A. Oswiecim ,Poland
Zinc Oxide	0.6	BASF AG, Germany
Stearic acid	1.5	BASF AG, Germany
Paraffin wax	1	Beesworks, China
TMQ	0.5	JSC Khimprom, Russia
TMTD	1	Taizhou Huangyan Donghai Chemical Co., Ltd., China
DOP	6	TIANHAO, China
Sulfur	2	BASF AG, Germany
Chlorophyll	20	Laboratory prepared
TiO ₂	20	Wuxi CHTI New Materials Co., Ltd., China
Nano-lead ratio	50,100,150,200,300	American Elements, USA

2.2. Radiation-shielding characterizations

Gamma radiation, a form of electromagnetic radiation discovered by Paul Villard in 1900, exhibits energies ranging from 1 to 14 MeV and travels at the speed of light. A lead equivalence test (IEC 61331-3:2014) was conducted to evaluate the shielding sheet's effectiveness. This test measures the reduction in gamma ray intensity (dI), which is directly proportional to both the initial intensity (I) and the thickness (dx) of the shielding material [19]:

$$dI = -\mu_L I dx \quad (1)$$

Integrating this equation, we obtain the Lambert-Beer law [20] :

$$I = I_0 e^{-\mu_L x} \quad (2)$$

where:

I= the intensity of photons transmitted across some distance x

I₀= the initial intensity of photons

μ_L = is the linear attenuation coefficient, representing the relative decrease in the number of photons per unit thickness measured in cm⁻¹.

x= shielding thickness

Materials with a large atomic number are preferred for manufacturing special gamma ray shields, and lead is considered the first material for gamma ray shielding.

The half-thickness is the thickness required to reduce the intensity to half of its original value:

$$\frac{1}{2}I_0 = I_0 e^{-\mu x_{1/2}} \quad (3)$$

$$\mu = (0.693/x_{1/2}) \quad (4)$$

The mass absorption coefficient data provided by Hubbell was utilized to determine the appropriate energy corresponding to the half-value layer for a specific energy level. This method was employed to pinpoint the most effective energy for optimal utilization [21]. The samples were exposed to gamma rays emitted by a Cobalt-60 source, which has an average energy of 1.25 MeV [22-24]

The linear attenuation coefficient can be represented as:

$$\mu_L = \frac{-\ln(I/I_0)}{x} \quad (5)$$

The relationship between the mass attenuation coefficient (μ_m) and the linear attenuation coefficient can be expressed as:

$$\mu_m = \frac{\mu_L}{\rho} \quad (6)$$

where ρ is the shielding material density.

The average distance between successive photon interactions, known as the mean free path (MFP), can be determined using the following formula: μ (in cm^{-1}) represents the linear attenuation coefficient.

$$MFP = 1/\mu_m \quad (7)$$

Rubber compound absorbance or reduction of gamma radiation intensity to half at a given energy is measured using the half-value layer (HVL). The relationship below is used to calculate the HVL [14]:

$$HVL = \ln 2/\mu_L \quad (8)$$

The gamma radiation attenuation coefficient is computed and proportional to the intensity decreasing to a tenth at a specific energy. Based on the relationship below, one can compute the tenth value layer (TVL) [25]:

$$TVL = \ln 10/\mu_L \quad (9)$$

2.3 Characterizations of the prepared samples

Various analytical techniques were employed to evaluate the prepared samples' characteristics. Scanning electron microscopy (CARL ZEISS ULTRA PLUS GEMINI FESEM) was used to examine the dispersion of lead nanoparticles within the rubber blends and to detect any surface agglomerations. Fourier transform infrared (FT-IR) spectroscopy (IRAffinity-1 S, Shimadzu, Japan) was utilized to analyze the chemical interactions among the components of the prepared samples.

The crystalline properties of the samples were investigated using X-ray diffraction (Rigaku Ultima-IV). The linear attenuation coefficient of the rubber compounds for gamma rays emitted by a Co-60 source (1.25 MeV) was measured using a digital LED display gamma-ray spectrometer

(EG&G Ortec DSPEC-USA). Furthermore, the density of the rubber compounds was determined with a DM 3000 density tester (ManTech, USA) in accordance with ASTM D297 standards.

3. Results and discussion

3.1. XRD analysis

The XRD analysis of natural rubber samples with varying lead concentrations revealed that the sample containing 50 pphr Pb exhibited the lowest intensity peaks. This indicates it possesses a lower degree of crystallinity than the other samples. For the 100 pphr Pb sample, slightly higher intensity and broader peaks are observed, indicating an increase in crystallinity, as shown in Figure 1. At 200 pphr Pb, even enhanced and sharper diffraction peaks occur for the sample, showing a higher structural order within the material. The sample with the highest lead content of 300 pphr shows the most intense and well-defined peaks. This confirms the strongest crystalline nature in the series. Therefore, the crystallinity of the natural rubber composites progressively increases with increasing lead concentration from 50 to 300 pphr based on changes in the peak profiles. The lead acts as a filler, strengthening the rubber matrix through physical interactions, limiting mobility and allowing denser packing of the polymer chains in crystalline lamellae. This gives natural rubber harder and stiffer properties with increased lead loading levels, as demonstrated by XRD analysis. The increasing lead concentration in the natural rubber composites significantly influenced the formation of crystalline domains through their interactions at the molecular level. As more lead particles were incorporated, they directly controlled polymer movements by imposing physical constraints. By dispersing and binding across numerous chain segments, the reinforcing lead fillers spatially limited the vibrations and fluctuations of these segments. This enabled optimized sequencing depending on the amount of filler by controlling cooperative movements into preferred orientations for crystallization. With additional lead loading, more excellent containment and direction could be achieved as the intervention potential multiplied. Chains experienced increased cooperative leadership toward closer cohesion within the lamella blades. The addition of nano-Pb can convert the amorphous phase to the crystalline phase due to molecular diffusion during the treatment [26]. Such concentration-dependent effects correlate with the systematically sharper XRD patterns, indicating increased structural regularity attributed to the dose-tuned modulation of the chain cooperativity of the fillers. The optimized structuring reached its peak at the highest tested load.

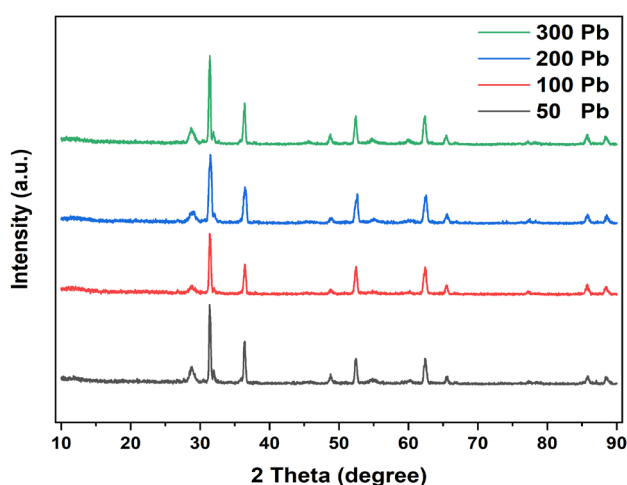


Fig. 1. XRD of the sample with different concentrations of Pb.

3.2. FTIR result

Fourier transform infrared spectroscopy (FTIR) was conducted to analyze the functional groups in SBR with varying lead ions (Pb) concentrations, as illustrated in Figure 2. The FTIR spectra for both untreated SBR and Pb-loaded SBR displayed absorption bands in the 4000–400 cm^{-1} range. Prominent peaks for pure SBR were observed at 3600 cm^{-1} , 2988 cm^{-1} , 2867 cm^{-1} , 1653 cm^{-1} , 1455 cm^{-1} , and 840 cm^{-1} .

The peaks at approximately 2988 cm^{-1} and 2867 cm^{-1} were attributed to the symmetric stretching of CH bonds [27]. The broad peak at 3600 cm^{-1} corresponds to O-H stretching vibrations, typically associated with alcohols, phenols, and carboxylic acids found in SBR biopolymers [28]. A weak absorption at 1733 cm^{-1} was identified as carbonyl (C=O) stretching of non-ionic carboxylic groups such as -COOH and -COOCH₃, indicating the presence of carboxylic acids and their esters. Previous studies suggest that carboxyl and hydroxyl groups in SBR biopolymers can interact with metal ions via adsorption processes [29].

The peak at 1640 cm^{-1} was also attributed to C=C stretching, characteristic of alkenes. The peak at 1280 cm^{-1} corresponds to C–O stretching, while the peak at 1026 cm^{-1} represents C–O stretching associated with ester groups. Finally, a peak near 1140 cm^{-1} was assigned to the Pb–O stretching linkage, demonstrating interactions between the rubber matrix and lead ions [30]. The ratio of absorptions at 840 cm^{-1} (assigned to =C–H wagging vibrations) and other peaks is frequently used in the fingerprint region for SBR characterization [31, 32]. With increasing Pb concentration, shifting of some peak positions was noticed, attributed to the interaction between Pb ions and carboxylate/hydroxylate groups on SBR through coordination bonding.

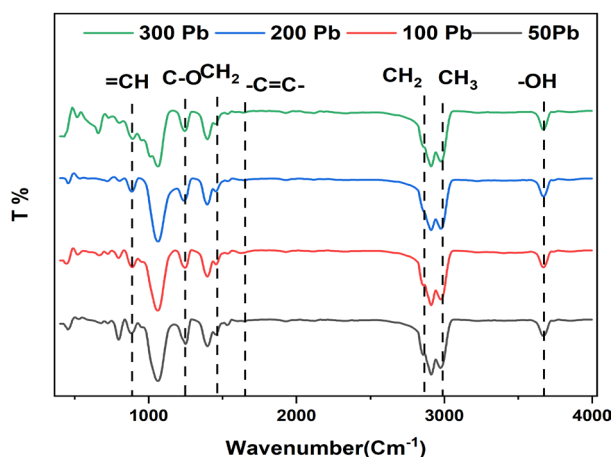


Fig. 2. FTIR of SBR sample with different concentrations of Pb.

3.3 Microstructure analysis

The microstructural characteristics of the silicone rubber nanocomposites with varying lead nanoparticle (N-Pb) concentrations were analyzed, as shown in Figure 3, using 60K magnification. The structural morphology of nanocomposite materials is influenced by several factors, including the type of filler, particle shape, particle size, filler selection, segment proportions, softening viscosities of segments, and manufacturing conditions [33].

As shown in Figure 3, the lead nanoparticles appear to be evenly distributed within the silicone rubber matrix, though some agglomeration and flaky structures are also visible. Increasing the concentration of lead nanoparticles led to an improvement in the homogeneity of the dispersion. Additional dough rolling was performed to reduce lead agglomeration; however, a lump of lead was still observed on the surface of the pressed samples. The uniform distribution of lead nanoparticles improves the mechanical properties and enhances the gamma-ray shielding efficiency of the rubber samples. The increased homogeneity also resulted in a more considerable cutting distance and final force, indicating improved mechanical properties [27, 34]. However, at higher nanoparticle loadings

(Figure 3d), the dispersion of nanoparticles transitions into aggregate structures. This aggregation at elevated loadings restricts the interaction between the polymer matrix and filler particles, ultimately causing filler sedimentation [35, 36].

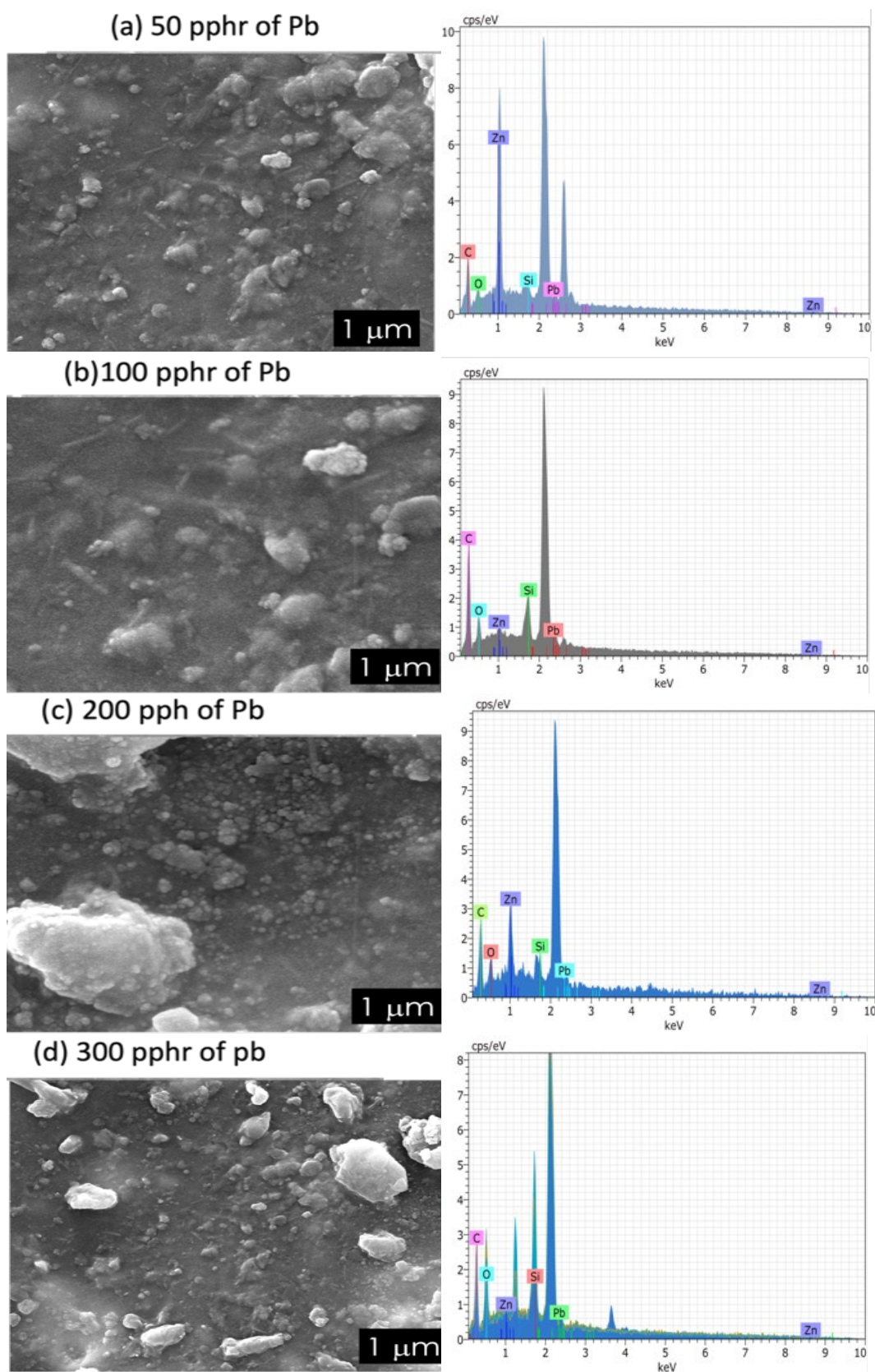


Fig. 3. SEM images of the prepared samples.

3.4. Gamma ray attenuation results

The gamma-ray attenuation properties of the rubber batch were investigated using varying ratios of lead (Pb) nanoparticles, as detailed in Table 2. The experimental setup included a shielding thickness of 0.3 cm and a distance of 30 cm from the cobalt-60 (Co-60) source to the sample.

Table 2. Linear and mass attenuation coefficients for different nano lead ratios.

Nano lead N-Pb ratio in(pphr)	0	50	100	150	200	300
Gamma Count rate (CPM)	736	610	560	543	520	501
Mass density(ρ_m (gm/cm^3))	1.0032	1.0059	1.5511	1.7821	2.0075	2.7775
linear attenuation coefficient(μ_L (cm^{-1}))	0.2966	0.6259	0.9109	1.0137	1.1580	1.2820
Mass attenuation coefficient(μ_m (cm^2/gm))	0.2956	0.6918	0.5873	0.5688	0.5768	0.4616
Mean free path (MFP)	3.3715	1.5976	1.0978	0.9865	0.8635	0.7800
Half value layer (HVL)	2.3369	1.1074	0.7609	0.6837	0.5985	0.5406
Tenth value layer (TVL)	7.7629	3.6787	2.5277	2.2713	1.9883	1.7960

The results demonstrate a clear relationship between the concentration of Pb nanoparticles and the gamma-ray attenuation characteristics of the rubber batch. As the ratio of nano lead increases from 0 to 300 pphr, there is a notable decrease in the gamma count rate, indicating enhanced attenuation. Specifically, a 31.9% reduction in the gamma count rate was observed when comparing the sample with no nano lead (736 cpm) to the sample with 300 pphr of nano lead (501 cpm). This inverse relationship is expected due to the lead's effectiveness as a gamma radiation absorber. Higher N-Pb ratios lead to increased attenuation and a lower measured count rate. The mass density also decreases with decreasing N-Pb ratio, as incorporating nano lead particles increases the overall density. Similarly, the linear attenuation coefficient (μ_L) decreases with increasing nano lead content; a 51.2% decrease was observed from 1.2820 cm^{-1} at 0 pphr to 0.6259 cm^{-1} at 50 pphr. This further supports the improved gamma radiation attenuation with increased nano lead content.

The mass attenuation coefficient (μ_m) also decreases with higher nano lead concentrations; it falls from $0.6918\text{ cm}^2/\text{g}$ at 0 pphr to $0.4616\text{ cm}^2/\text{g}$ at 300 pphr, reflecting a 33.2% reduction. The linear attenuation coefficient quantifies how the beam intensity decreases exponentially with thickness, so higher μ_L values indicate more attenuation per unit thickness. The trend of increasing μ_L with lower N-Pb ratios matches the density and count rate trends.

Similarly, the mass attenuation coefficient, which normalizes for differences in density, still increases with lower N-Pb ratios within the range of densities measured. This suggests that lead is the primary attenuating element. The MFP decreases approximately from the lowest to the highest lead concentration, and these results agree with those of a previous study [37, 38]. This reduction in MFP indicates a shorter mean distance traveled by gamma rays before interaction with lead nanoparticles. Furthermore, the half-value layer (HVL) and tenth-value layer (TVL) demonstrate significant reductions (approximately 77% and 87%, respectively) with increasing lead concentration. This enhanced attenuation efficiency is attributed to the high density and atomic number of lead, significantly increasing the material's absorption capacity. The decrease in HVL and TVL, representing the thicknesses required to reduce radiation intensity by half and one-tenth, respectively, directly confirms the improved shielding performance of the composite material [39].

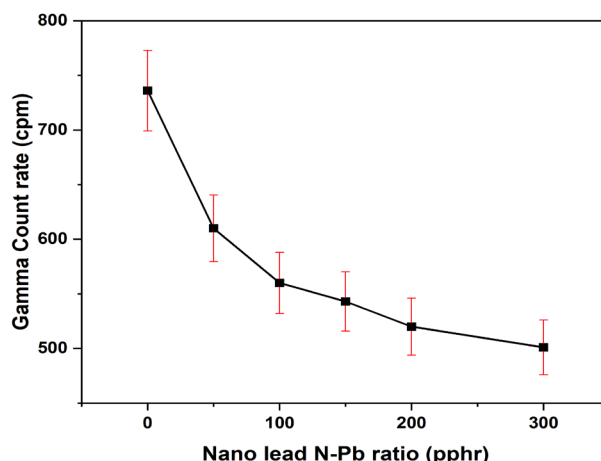


Fig. 4. Effect of Nano lead (PPhr) on the intensity of absorption gamma radiation.

Figure 4 illustrates the inverse relationship between gamma radiation intensity and nano-lead concentration (pphr), demonstrating the attenuating effect of lead nanoparticles. This observation supports the potential application of lead-containing materials, such as lead-powder-filled rubber gloves, for radiation shielding in environments with high ionizing radiation exposure, like cancer treatment facilities, to enhance the protection of medical personnel. The calculation rate of gamma radiation emitted from a cobalt source (Co-60) with different thicknesses has been measured and shown in Table 3.

Table 3. The compounds of rubber with 300pphr Pb have different shielding thicknesses.

shield	Thickness X (cm)	Gamma Count rate(cpm)	Gamma Count rate(cps)	Ln(I/I ₀)
SBR+ nano Pb shield	0	736	12.26	0
	0.15	673	11.21	-0.089
	0.2	625	10.41	-0.163
	0.3	501	8.35	-0.384
	0.4	425	7.08	-0.549

The results in Table 3 show the attenuating gamma radiation by examining the gamma count rate in counts per second (cps) and counts per minute (CPM) as a function of shield thickness. The results reveal that the gamma count rate decreases significantly with increasing shield thickness, indicating the shield's effectiveness in attenuating gamma radiation. Specifically, the gamma count rate drops from 736 cpm (12.26 cps) with no shielding to 425 cpm (7.08 cps) at a shield thickness of 0.4 cm, representing a 42.3% reduction in the gamma count rate. Additionally, the logarithmic attenuation ($\ln(I/I_0)$) shows a marked increase as the shield thickness increases, starting at 0 with no shielding and increasing to -0.549 at a thickness of 0.4 cm.

The most significant change in logarithmic attenuation occurs between 0.2 cm and 0.3 cm of shield thickness, with $\ln(I/I_0)$ increasing by 135.6% from -0.163 to -0.384, reflecting improved shielding efficiency at larger thicknesses of exponential attenuation illustrates behavior described by Beer's law, in which the intensity decreases in proportion to the thickness and the attenuation coefficient. Even the most negligible thickness of 0.15 cm results in measurable attenuation. Notably, doubling the thickness from 0.2 cm to 0.4 cm almost halves the count rate, indicating the dramatic additional shielding effect of even a slight increase in thickness. A semi-logarithmic plot of $\ln(I/I_0)$ versus thickness shows an approximately linear relationship, confirming that Beer's law accurately models' attenuation across the tested thicknesses. An exponential increase in thickness

improves the gamma-ray attenuation capabilities of this composite shielding material and demonstrates its effectiveness even at small thicknesses for shielding applications [40, 41]. The gamma count rate values are plotted with shield thicknesses $X(\text{cm})$, as shown in Figure 5.

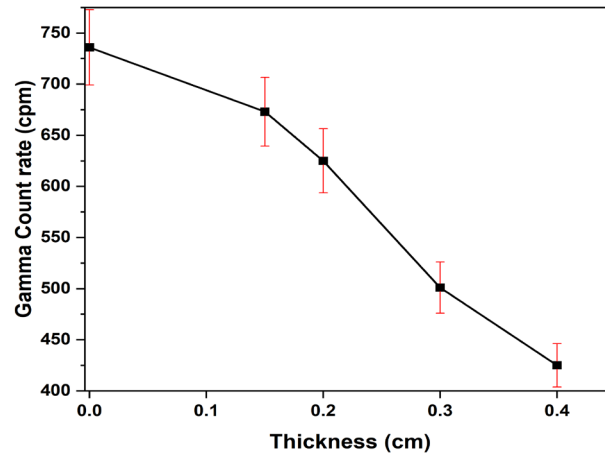


Fig. 5. Relationship between gamma count rate (cpm) and material thickness (cm).

The values of $\ln \frac{I}{I_0}$ with shielding thicknesses $X(\text{cm})$ are shown in Figure 6.

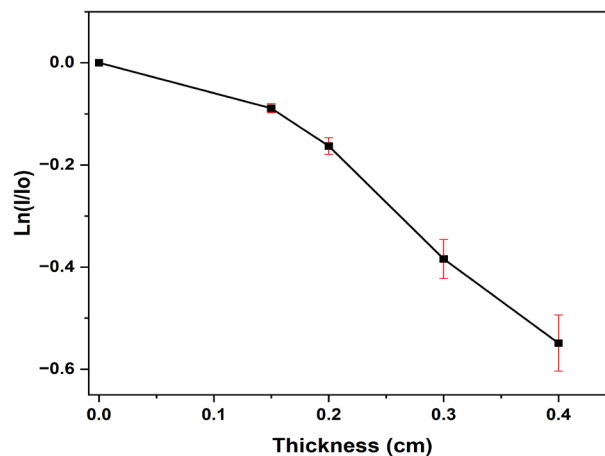


Fig. 6. Gamma count rate as a function of material thickness.

The slope of the linear damping coefficient is determined to be $\mu_L = 1.015 \text{ cm}^{-1}$. This indicates that the material predominantly absorbs the incident gamma radiation, as evidenced by a linear absorption coefficient of 0.1. When the absorption coefficient approaches zero, the material exhibits transparency to radiation; conversely, as the absorption coefficient increases towards unity, the material's capacity to absorb radiation increases significantly. It is important to note that the measured value of the linear attenuation coefficient exceeds internationally published values, which are contingent upon the overall attenuation coefficient derived from the combined effects of gamma-ray interactions, including the photoelectric effect, Compton scattering, and pair production. Figure 7 illustrates that the linear attenuation coefficients increase with the proportion of nano-lead particles. The optimal ratio for radiation shielding is identified as 300 pphr, making it the most effective composition for gamma-ray attenuation.

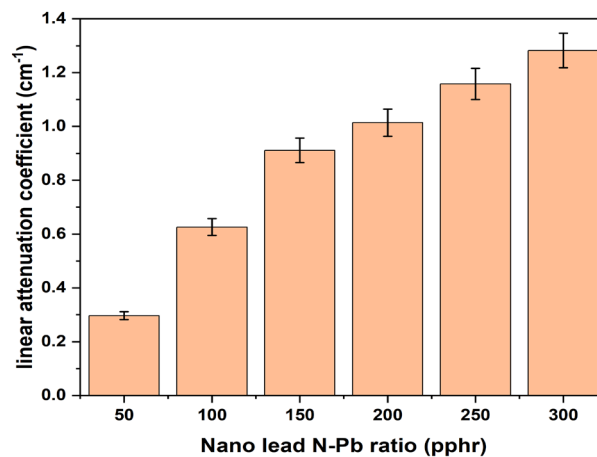


Fig. 7. The relation between linear attenuation coefficient and Nano lead in(pphr)unit.

Figure 8 shows an inverse relationship between mass attenuation coefficient and nano-lead concentration. This trend is attributed to the increase in mass density resulting from the higher proportion of nanoparticles.

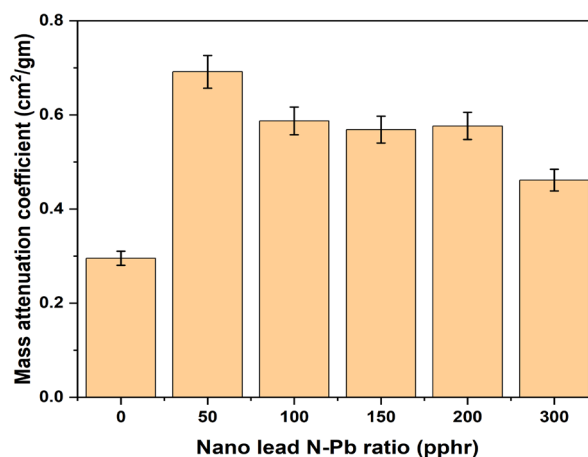


Fig. 8. Effect of Nano Lead (N-Pb) Ratio on Mass Attenuation Coefficient.

Lead has a high atomic number of 82, which contains many electrons that can interact with incident gamma rays [42]. Gamma rays are most likely to interact with materials via the photoelectric effect or Compton scattering, and these interaction probabilities increase with the number of electrons in an atom. Lead also has a high density of 11.34 g/cm^3 , so many atoms are tightly packed in a small volume. This increases the likelihood of gamma-ray interactions because more radiation must pass through more atoms in a given material thickness [43]. In addition, lead contains K-shell electrons with absorption edges around 88 keV, corresponding to the usual gamma-ray energies of radioactive sources such as cobalt-60 and cesium-137 [44]. Likely, the photoelectric effect entirely absorbs gamma rays at or below these energies. Due to its high atomic number, density, and practical absorption edges, lead exhibits excellent shielding ability over a wide gamma-ray energy range from about 30 keV to over 1 MeV. Even thin layers of lead can absorb most of the incident gamma rays. These material properties give lead uniquely good properties for stopping gamma rays through dominant photoelectric and Compton interactions, making it a preferred material for applications requiring gamma radiation shielding.

4. Conclusions

This study demonstrates the successful enhancement of gamma radiation shielding properties in styrene-butadiene rubber (SBR) by incorporating lead nanoparticles. A significant reduction in gamma count rate (31.9%) was observed with increasing nano-lead (N-Pb) concentration (50-300 pphr), confirming improved attenuation. This improvement is corroborated by the enhanced linear (μL) and mass (μm) attenuation coefficients at higher N-Pb loadings. Furthermore, the decreased mean free path, half-value layer, and tenth-value layer directly indicate reduced gamma ray penetration depth. The uniform nanoparticle distribution within the SBR matrix contributes to improved mechanical properties and enhanced shielding efficacy. These findings highlight the potential of the developed SBR-N-Pb composite for effective gamma radiation protection in diverse applications, including healthcare and nuclear industries, warranting further investigation into its long-term stability and scalability for practical implementation.

References

- [1] W.I. Luining, M.C. Cysouw, D. Meijer, N.H. Hendrikse, R. Boellaard, A.N. Vis, D.E. Oprea-Lager, *Cancers (Basel)* 14(5) (2022) 1169; <https://doi.org/10.3390/cancers14051169>
- [2] E. Russ, C.M. Davis, J.E. Slaven, D.T. Bradfield, R.G. Selwyn, R.M. Day, *Toxics* 10(10) (2022) 628; <https://doi.org/10.3390/toxics10100628>
- [3] K. Koka, A. Verma, B.S. Dwarakanath, R.V. Papineni, *Cancer Manag. Res.* 14 (2022) 1421-1429; <https://doi.org/10.2147/CMAR.S351744>
- [4] A. Montoro, E. Obrador, D. Mistry, G.I. Forte, V. Bravatà, L. Minafra, M. Calvaruso, F.P. Cammarata, M. Falk, G. Schettino, *Radioprotectors, Radiomitigators, and Radiosensitizers, Radiobiology Textbook*, Springer2023, pp. 571-628; https://doi.org/10.1007/978-3-031-18810-7_11
- [5] Q. Chang, S. Guo, X. Zhang, *Mater. Des.* 233 (2023) 112253; <https://doi.org/10.1016/j.matdes.2023.112253>
- [6] A. Hamisu, O. Khiter, S. Al-Zhrani, W.S.B. Haridh, Y. Al-Hadeethi, M. Sayeed, S. Tijani, *Radiat. Phys. Chem.* 216 (2023) 111448; <https://doi.org/10.1016/j.radphyschem.2023.111448>
- [7] S. Ashley, *Sci Am.* 288(5) (2003) 34-35; <https://doi.org/10.1038/scientificamerican0503-34>
- [8] O. Kilicoglu, C.V. More, F. Akman, K. Dilsiz, H. Oğul, M.R. Kaçal, H. Polat, O. Agar, *Radiat. Phys. Chem.* 194 (2022) 110039; <https://doi.org/10.1016/j.radphyschem.2022.110039>
- [9] M.H. Naeem, S.H.H. Al-Nesrawy, M.H. Al-Maamori, *EEJP* (3) (2023) 539-545; <https://doi.org/10.26565/2312-4334-2023-3-63>
- [10] I.J. H, *Journal of University of Babylon* 17(1) (2009).
- [11] S. Nambiar, E.K. Osei, J.T. Yeow, *J. Appl. Polym. Sci.* 127(6) (2013) 4939-4946; <https://doi.org/10.1002/app.37980>
- [12] S.M. Badawy, A. Abd El-Latif, *Polym. Compos.* 38(5) (2017) 974-980; <https://doi.org/10.1002/pc.23660>
- [13] A.K. Aobaid, Y. Taha, S. Al_qaisy, *Journal of Physics: Conference Series*, IOP Publishing, 2020, p. 012021; <https://doi.org/10.1088/1742-6596/1664/1/012021>
- [14] A.M. El-Khatib, M.I. Abbas, S.I. Hammoury, M.M. Gouda, K. Zard, M. Elsafi, *Sci. Rep.* 12(1) (2022) 15722; <https://doi.org/10.1038/s41598-022-20103-z>
- [15] R.A.A.K. Abbas, M.H.A. Maamori, *AIP Conf. Proc.*, AIP Publishing, 2023; <https://doi.org/10.1063/5.0129387>
- [16] V. Harish, N. Nagaiah, H. Kumar, *IJPAP* 50 (2012) 847-850.
- [17] A. Mheemeed, H. Hasan, F. Al-Jomaily, *J. Radioanal. Nucl. Chem.* 291(3) (2012) 653-659; <https://doi.org/10.1007/s10967-011-1556-2>

- [18] F.K. Dahash, A.K. Aobaid, M.H. Al Maamori, Egypt. J. Chem. 65(1) (2022) 91-94.
- [19] L.R. Dartnell, Astrobiology. 11(6) (2011) 551-582; <https://doi.org/10.1089/ast.2010.0528>
- [20] N. Tsoulfanidis, S. Landsberger, CRC press, 2021; <https://doi.org/10.1201/9781003009849>
- [21] S.-C. Kim, K.-R. Dong, W.-K. Chung, Ann. Nucl. Energy 47 (2012) 1-5; <https://doi.org/10.1016/j.anucene.2012.04.014>
- [22] A. El-Sersy, A. Hussein, H. El-Samman, N. Khaled, A. El-Adawy, H. Donya, J. Radioanal. Nucl. Chem. 288(1) (2011) 65-69; <https://doi.org/10.1007/s10967-010-0924-7>
- [23] M.J. Alduhaibat, M.S. Amana, A.J. Farhan, N.J. Jubier, IOP Publishing, 2020, p. 012013; <https://doi.org/10.1088/1757-899X/757/1/012013>
- [24] M.M.H. Baba, M. Mohib-ul-Haq, M.A.A. Khan, Int. J. Health Sci. 7(1) (2013) 15; <https://doi.org/10.12816/0006016>
- [25] P.S. Dahinde, G. Dapke, S. Raut, R. Bhosale, P.P. Pawar, Indian J. Sci. Res. 9(2) (2019) 79-84; <https://doi.org/10.32606/IJSR.V9.I2.00014>
- [26] N. Bukit, E. Frida, Makara j.technol 17(3) (2013) 3; <https://doi.org/10.7454/mst.v17i3.2926>
- [27] R. Gamal, E. Salama, M. Ehab, D.E. El-Nashar, A. Bakry, AIP Conf. Proc., AIP Publishing, 2023; <https://doi.org/10.1063/5.0120701>
- [28] M. Iqbal, A. Saeed, S.I. Zafar, J. Hazard. Mater. 164(1) (2009) 161-171; <https://doi.org/10.1016/j.jhazmat.2008.07.141>
- [29] R. Ashkenazy, L. Gottlieb, S. Yannai, Biotechnol. Bioeng. 55(1) (1997) 1-10; [https://doi.org/10.1002/\(SICI\)1097-0290\(19970705\)55:1<1::AID-BIT1>3.0.CO;2-H](https://doi.org/10.1002/(SICI)1097-0290(19970705)55:1<1::AID-BIT1>3.0.CO;2-H)
- [30] S. Atef, D.E. El-Nashar, A. Ashour, S. El-Fiki, S. El-Kameesy, M. Medhat, Polym. Bull. 77 (2020) 5423-5438; <https://doi.org/10.1007/s00289-019-03022-4>
- [31] M. Arroyo, M. Lopez-Manchado, B. Herrero, Polym. 44(8) (2003) 2447-2453; [https://doi.org/10.1016/S0032-3861\(03\)00090-9](https://doi.org/10.1016/S0032-3861(03)00090-9)
- [32] S. Gunasekaran, R. Natarajan, A. Kala, Spectrochim. Acta - A: Mol. Biomol. Spectrosc. 68(2) (2007) 323-330; <https://doi.org/10.1016/j.saa.2006.11.039>
- [33] S. Al-Janabi, M. Al-Maamori, A. Braihi, IOP Conference Series: Materials Science and Engineering, IOP Publishing, 2021, p. 012150; <https://doi.org/10.1088/1757-899X/1094/1/012150>
- [34] S. Intom, E. Kalkornsurapranee, J. Johns, S. Kaewjaeng, S. Kothan, W. Hongtong, W. Chaiphaksa, J. Kaewkhao, Radiat. Phys. Chem. 172 (2020) 108772; <https://doi.org/10.1016/j.radphyschem.2020.108772>
- [35] M.A. Sanjari Shahrezaei, F. Goharpey, R. Foudazi, Polym. Compos. 39(8) (2018) 2904-2914; <https://doi.org/10.1002/pc.24287>
- [36] M. Ramesh, L.N. Rajeshkumar, N. Srinivasan, D.V. Kumar, D. Balaji, e-Polymers 22(1) (2022) 898-916; <https://doi.org/10.1515/epoly-2022-0080>
- [37] A.M. Ali, M.I. Sayyed, M. Rashad, A. Kumar, R. Kaur, A. Aşkın, H. Algarni, Appl. Phys. A 125(10) (2019) 671; <https://doi.org/10.1007/s00339-019-2964-3>
- [38] A. Elazaka, H.M. Zakaly, S.A. Issa, M. Rashad, H. Tekin, H. Saudi, V. Gillette, T. Erguzel, A. Mostafa, J. Hazard. Mater. 403 (2021) 123738; <https://doi.org/10.1016/j.jhazmat.2020.123738>
- [39] M. Erdem, O. Baykara, M. Doğru, F. Kuluöztürk, Radiat. Phys. Chem. 79(9) (2010) 917-922; <https://doi.org/10.1016/j.radphyschem.2010.04.009>
- [40] R. Li, Y. Gu, Z. Yang, M. Li, Y. Hou, Z. Zhang, Mater. Des. 124 (2017) 121-130; <https://doi.org/10.1016/j.matdes.2017.03.045>
- [41] A.E.-S. Abdo, M. Ali, M. Ismail, Radiat. Phys. Chem 66(3) (2003) 185-195; [https://doi.org/10.1016/S0969-806X\(02\)00470-X](https://doi.org/10.1016/S0969-806X(02)00470-X)
- [42] B. Oto, S.E. Gulebaglan, Z. Madak, E. Kavaz, Radiat. Phys. Chem. 159 (2019) 195-206; <https://doi.org/10.1016/j.radphyschem.2019.03.010>

- [43] I.M. Low, N.Z.N. Azman, Polymer composites and nanocomposites for X-rays shielding, Springer2020; <https://doi.org/10.1007/978-981-13-9810-0>
- [44] J. Allison, Aust. J. Phys. 14(4) (1961) 443-468; <https://doi.org/10.1071/PH610443>